

## Research Paper

## Fine-scale perspectives on landscape phenology from unmanned aerial vehicle (UAV) photography



Stephen Klosterman<sup>a,\*</sup>, Eli Melaas<sup>b</sup>, Jonathan A. Wang<sup>b</sup>, Arturo Martinez<sup>c</sup>, Sidni Frederick<sup>c</sup>, John O'Keefe<sup>c</sup>, David A. Orwig<sup>c</sup>, Zhuosen Wang<sup>d,e,f</sup>, Qingsong Sun<sup>d</sup>, Crystal Schaaf<sup>d</sup>, Mark Friedl<sup>b</sup>, Andrew D. Richardson<sup>a,g,h</sup>

<sup>a</sup> Department of Organismic and Evolutionary Biology, Harvard University, 26 Oxford St, Cambridge, MA 02138, USA

<sup>b</sup> Earth and Environment, Boston University, 685 Commonwealth Avenue, Boston, MA 02215, USA

<sup>c</sup> Harvard Forest, Harvard University, 324 N Main St, Petersham, MA 01366, USA

<sup>d</sup> School for the Environment, University of Massachusetts Boston, 100 William T Morrissey Blvd, Boston, MA 02125, USA

<sup>e</sup> Terrestrial Information Systems Laboratory, NASA Goddard Space Flight Center, 8800 Greenbelt Rd, Greenbelt, MD 20771, USA

<sup>f</sup> Earth System Science Interdisciplinary Center, University of Maryland, 5825 University Research Ct, College Park, MD 20740, USA

<sup>g</sup> School of Informatics, Computing, and Cyber Systems, Northern Arizona University, 1514 S Riordan Ranch St, Flagstaff, AZ 86011, USA

<sup>h</sup> Center for Ecosystem Science and Society, Northern Arizona University, P.O. Box 5620, Flagstaff, AZ 86011, USA

## ARTICLE INFO

## Keywords:

Phenology

Forest

Spatial scaling

Unmanned aerial vehicle (UAV)

Drone

Satellite remote sensing

## ABSTRACT

Forest phenology is a multi-scale phenomenon, arising from processes in leaves and trees, with effects on the ecology of plant communities and landscapes. Because phenology controls carbon and water cycles, which are commonly observed at the ecosystem scale (e.g. eddy flux measurements), it is important to characterize the relation between phenophase transition events at different spatial scales. We use aerial photography recorded from an unmanned aerial vehicle (UAV) to observe plant phenology over a large area (5.4 ha) and across diverse communities, with spatial and temporal resolution at the scale of individual tree crowns and their phenophase transition events (10 m spatial resolution, ~5 day temporal resolution in spring, weekly in autumn). We validate UAV-derived phenophase transition dates through comparison with direct observations of tree phenology, PhenoCam image analysis, and satellite remote sensing. We then examine the biological correlates of spatial variance in phenology using a detailed species inventory and land cover classification. Our results show that species distribution is the dominant factor in spatial variability of ecosystem phenology. We also explore statistical relations governing the scaling of phenology from an organismic scale (10 m) to forested landscapes (1 km) by analyzing UAV photography alongside Landsat and MODIS data. From this analysis we find that spatial standard deviation in transition dates decreases linearly with the logarithm of increasing pixel size. We also find that fine-scale phenology aggregates to a coarser scale as the median and not the mean date in autumn, indicating coarser scale phenology is less sensitive to the tails of the distribution of sub-pixel transitions in the study area. Our study is the first to observe forest phenology in a spatially comprehensive, whole-ecosystem way, yet with fine enough spatial resolution to describe organism-level correlates and scaling phenomena.

## 1. Introduction

Forest phenology has gained wide recognition as a sensitive indicator of global change, and determines the timing of ecosystem processes that may elicit feedbacks within the earth system (Morissette et al., 2009; Polgar and Primack, 2011; Richardson et al., 2013). The advance of spring onset in temperate forests in recent decades (Ault et al., 2015; Miller-Rushing and Primack, 2008; Schwartz et al., 2006), and earlier canopy activity in the spring time, have been linked to

increased carbon sequestration in forest ecosystems (Badeck et al., 2004; Keenan et al., 2014b; Richardson et al., 2010). Autumn extension of the growing season has also been shown to increase net annual productivity (Dragoni et al., 2011; Keenan et al., 2014b). As understanding of the causal factors of forest phenology develops, both global scale observations from satellite remote sensing, and plot scale studies of trees, will play crucial roles in linking phenological processes to ecosystem function (Cleland et al., 2007; Ibáñez et al., 2010; Menzel et al., 2006; Morissette et al., 2009; Vitasse et al., 2009).

\* Corresponding author.

E-mail address: [steve.klosterman@gmail.com](mailto:steve.klosterman@gmail.com) (S. Klosterman).

Harmonizing such diverse scales of information presents distinct challenges to the characterization of phenology. Investigators rely on satellite remote sensing for a complete view of the earth system, but at the expense of spatial resolution, which is typically in the hundreds of meters for global phenology data (Cleland et al., 2007; Verger et al., 2016; White et al., 2009; Zhang et al., 2006, 2003). Discerning the plant physiological processes governing phenology transitions relies on plot scale observations and experiments with individuals, which must be scaled up to represent ecosystem processes (Jarvis, 1995; Stoy et al., 2009); heterogeneous landscapes, composed of diverse plant communities, complicate the scaling process (Doktor et al., 2009; Hufkens et al., 2012; Klosterman et al., 2014). Even within one plant community type, limited ground-based observations may not accurately represent variability in ecosystem dynamics, if there is significant microclimatic variation (Fisher and Mustard, 2007).

These challenges highlight the need for phenology observation at intermediate scales, such as the canopy scale of phenocams (Richardson et al., 2007). These tower-mounted digital cameras can be used to obtain high temporal resolution, near-surface phenology data, akin to the vegetation indices of satellite remote sensing (Huete et al., 2002; Verger et al., 2016). Phenophase transition dates estimated from digital images have been shown to correlate with plant life cycle features, such as spring budburst and autumn senescence, carbon assimilation, and leaf physiology parameters (Keenan et al., 2014a; Toomey et al., 2015; Wingate et al., 2015; Yang et al., 2014).

While the low cost and familiar technology of digital cameras makes the phenocam method popular (Brown et al., 2016), their stationary, tower-mounted perspective limits the area of observation. Aerial photography is a natural extension of the phenocam technique. The recent technological revolution in unmanned aerial vehicles (UAVs), also known as drones, makes it feasible to collect aerial images with the temporal resolution necessary to monitor plant phenology events (Anderson and Gaston, 2013; Berra et al., 2016; Dandois and Ellis, 2013; Lisein et al., 2015). A low cost approach is possible (total hardware and software cost ~\$2000), using a consumer grade digital camera mounted on a UAV, and photogrammetry software to create georeferenced mosaic images, similar to imagery available from platforms such as Google Maps. UAVs continue to find new applications in plant science and ecology, including detailed characterization of the 3D structure of individual tree crowns (Gatzolis et al., 2015), 3D structure and color properties of forest canopies (Dandois and Ellis, 2013), and micro-topography of Antarctic mosses (Lucieer et al., 2014). In the context of tree phenology, recent studies used UAV photography in a validation study showing that ground-based observations of spring budburst are correlated with individual tree-scale analyses of digital photography (Berra et al., 2016), and presented phenological analyses of individuals as a method for identifying tree species (Lisein et al., 2015).

Here, we use a lightweight UAV to identify spring and fall phenophase transition events on a landscape scale (5.4 ha area) corresponding to a MODIS pixel, with fine spatial resolution (10 m, dividing the MODIS pixel in to 540 micro-pixels). We break this area down into plant communities, and use a detailed map of tree species and *in-situ* phenology observations to explore variance between and within communities. Then, by using several resolutions of image analysis, as well as medium and coarse resolution remote sensing (Landsat and MODIS), we describe the nature of spatial scaling in phenophase transition dates. Specifically, we answer these questions:

- What is the timing of phenology events between and within plant communities in a mixed forest ecosystem (deciduous trees, evergreen trees, wetlands) and how do they scale up to aggregate measures of ecosystem phenology?
- What is the biological interpretation of phenophase transitions derived from UAV photography, and how well does *in-situ* observation of a small set of individuals (3–5) represent the larger deciduous

community?

- To what degree does spatial variation in phenology correlate to differences in species assemblage?
- What are the statistical relationships of landscape phenology transition dates across different spatial resolutions?

## 2. Methods

### 2.1. Study site

We conducted our study at Harvard Forest in Petersham, MA. The study area is a mixed deciduous-evergreen forest, with some woody wetlands, annual mean precipitation of 110 cm, and a temperate climate with mean annual temperature 7.1 °C. Deciduous trees in the study area include predominantly red oak (*Quercus rubra*) and red maple (*Acer rubrum*), but also yellow birch (*Betula alleghaniensis*), American beech (*Fagus grandifolia*), and black oak (*Quercus velutina*).

### 2.2. Digital image acquisition and processing

Within Harvard Forest, our primary study area was a 250 m MODIS pixel (ground area 5.4 ha) containing the PhenoCam mounted on the Environment Measurement Station tower (EMS; 42.5378, –72.1715; the ‘harvard’ PhenoCam, see <http://phenocam.sr.unh.edu/>). We obtained aerial photography over the primary study area using a UAV (3DR ArduCopter Quad-C Frame, 3D Robotics, Berkeley, CA) equipped with a Canon Powershot A3300 camera. The camera took photos continuously throughout each flight, using an intervalometer script programmed with the Canon Hack Development Kit (CHDK, <http://chdk.wikia.com/wiki/CHDK>). Images were taken at a minimum shutter speed of 1/1000 s, with constant exposure during each flight. The same color balance was used for all acquisition dates, as consistent color balance has been shown to be important for reliable digital camera observations of phenology (Richardson et al., 2009). We recorded images in the JPEG file format, as opposed to RAW, for faster image capture time and increased frequency of photos during flight. The utility of JPEGs for plant phenology study has been thoroughly demonstrated (Ahrends et al., 2008; Keenan et al., 2014a; Sonnentag et al., 2012; Toomey et al., 2015). We used the same camera and image settings for all flights, and took pictures of a gray reference square (ColorChecker classic, X-rite, Grand Rapids, MI) before each flight on all but the first date of image acquisition. Frequency of flights was roughly every five days during spring leaf out and every week during fall senescence and abscission in 2013, depending on weather conditions (acquisition dates shown in Fig. 1G). We programmed the UAV to fly between waypoints that covered the study area in two flights of approximately 10 min each (example flight logs shown in Fig. S1, with flight plan description in caption).

We combined camera imagery (~400 photos per acquisition date) into orthophotos covering the study area, using the PhotoScan software package (Agisoft, St. Petersburg, Russia). Initial estimates of camera location for each photo were derived from flight logs of the GPS on board the UAV, and timestamps of image files, using custom scripts written in Matlab (The Mathworks, Natick, MA). We used the following steps and options in PhotoScan:

1. Align Photos: Accuracy, High; Pair preselection, Ground Control; Point limit, 40000; Constrain features by mask, No.
2. Build Dense Cloud: Quality, Medium; Depth filtering, Moderate; Reuse depth maps, No.
3. Build Mesh: Surface type, Arbitrary; Source data, Dense cloud; Interpolation, Enabled; Face count, Medium.

We exported orthophotos from PhotoScan and performed final georeferencing in ERDAS IMAGINE AutoSync (Intergraph, Huntsville, AL) using aerial photography obtained from the Massachusetts Office of

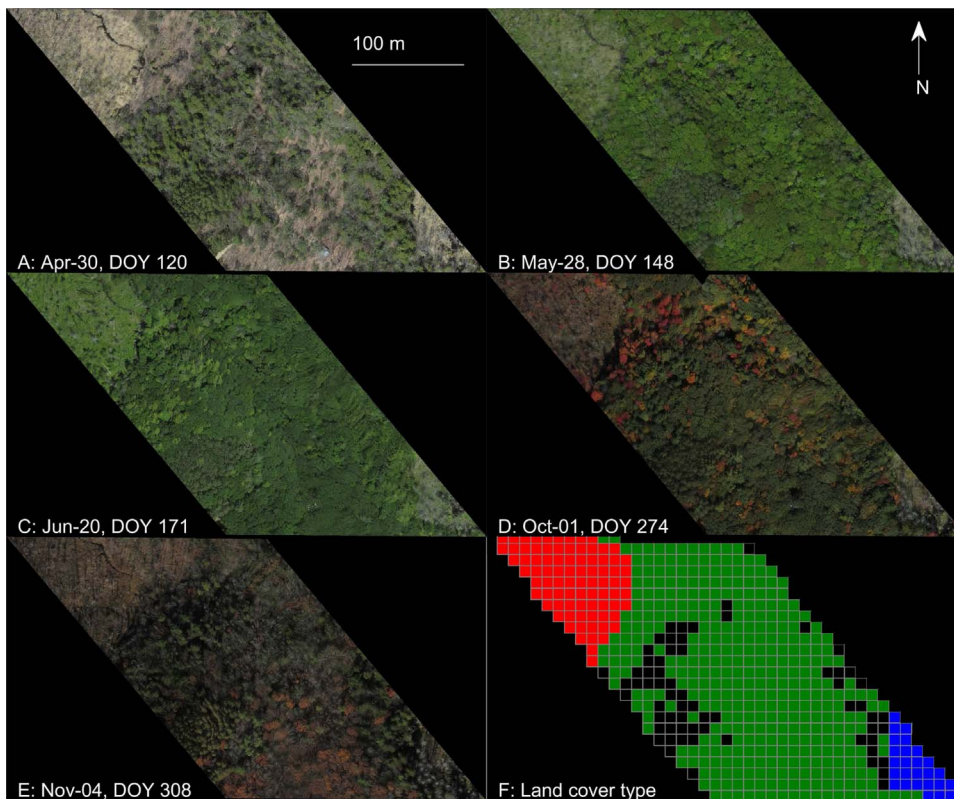
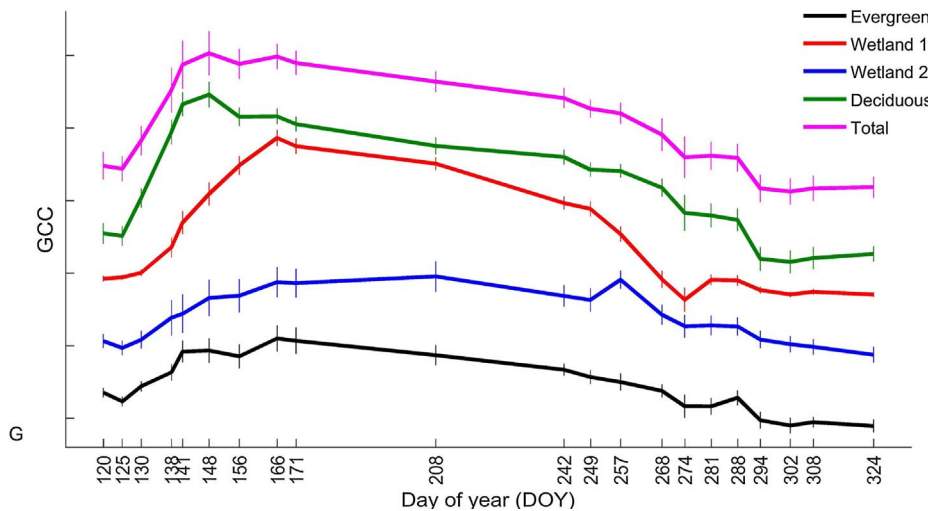


Fig. 1. A–E; Orthophotos from before (April 30), during (May 28), and after leaf out (June 20), and during senescence of red maples (October 1) and red oaks (November 4). F; A map showing the different plant communities (deciduous = green, wetlands = red and blue, evergreen = black). G; Green chromatic coordinate ( $G_{CC}$ ) from all dates of UAV photography, averaged over each community, as well as the entire study area.  $G_{CC}$  time series have been offset in the y direction for visibility; y-axis ticks are spaced at an interval of 0.02; most time series start at  $G_{CC} \approx 0.36$ , except for evergreen which starts at  $G_{CC} \approx 0.40$ . Vertical bars show one standard deviation. (For interpretation of the references to color in this figure legend, the reader is referred to the web version of this article.)



Geographic Information (MassGIS) to identify control points, consisting of large evergreen trees and other landscape features that were clearly visible. Orthophotos had a nominal resolution of 6 cm, however we noted errors in the spatial alignment of tree crowns across acquisition dates, likely arising from a number of sources including inaccuracy of the onboard GPS, wind-blown motion of trees, the automated orthophoto mosaicking process, and user error in final georeferencing. After comparing orthophotos from two acquisitions on the same date, and considering the nature of the species data, discussed further in Section 2.5, we decided to use a 10 m resolution as the finest scale for analysis. We obtained similar results when the analysis was repeated with 5 m and 3 m grids, and note that minimal additional spatial variance in phenology could be gained by using these resolutions.

To calculate phenology time series data from images, orthophotos were divided into regions of interest (ROIs) ranging in size from 10 m by 10 m, up to the entire study area. For each region of interest, we calculated time series of green chromatic coordinate ( $G_{CC}$ ):

$$G_{CC} = \frac{G}{R + G + B} \tag{1}$$

by averaging the red (R), green (G), and blue (B) digital numbers from the pixels in each ROI, on each acquisition date (Sonnentag et al., 2012). Example  $G_{CC}$  time series and additional details are available in Fig. S2 and its caption. A record of all orthophotos and flight logs is available in the Harvard Forest Data Archive at <http://harvardforest.fas.harvard.edu:8080/exist/apps/datasets/showData.html?id=hf294>.

### 2.3. Remote sensing of phenology

Surface reflectances were obtained from Landsat (48 by 48 grid of 30 m pixels, weekly temporal resolution) and MODIS (8 by 8 grid of 250 m pixels, daily temporal resolution) over 346 ha of mixed deciduous-evergreen forest, containing the primary study area, for 2013. This larger area encompasses much of the Prospect Hill tract of Harvard

Forest, and some of the surrounding forested land.

Following the methods of Melaas et al. (2013), we used a 30 year time series of Landsat images to identify spring and autumn phenology dates. Since Landsat phenology data was scarce at Harvard Forest in 2013, due to cloud cover on acquisition dates during leaf-out, we used the closest year with good data availability and similar phenology based on PhenoCam data, which was 2008. However we also conducted analysis using other nearby years with good data availability (2009, 2010, and 2011) and obtained similar results. We used the enhanced vegetation index (EVI), a proxy of photosynthetic activity (Huete et al., 2002), for calculating Landsat phenology:

$$EVI = \frac{2.5(\rho_{NIR} - \rho_R)}{(\rho_{NIR} + 6\rho_R - 7.5\rho_B + 1)} \quad (2)$$

where  $\rho_{NIR}$ ,  $\rho_R$ , and  $\rho_B$  are reflected light in the near-infrared, red, and blue bands, respectively. MODIS data were obtained from the Nadir BRDF Adjusted Reflectance (NBAR) product, custom prepared at 250 m resolution as a daily retrieval for this study (Shuai et al., 2013). We used only data flagged as “high quality” and with no snow present, according to quality control products contained along with MODIS NBAR surface reflectance data (Campagnolo et al., 2016; Schaaf et al., 2008, 2002, 2011), and calculated EVI similar to Landsat, as well as  $G_{CC}$  similar to Eq. (1). For the Landsat surface reflectance and MODIS NBAR data, we explored additional spatial resolutions by averaging reflectances over aggregates of 2 by 2, 4 by 4, etc. groups of pixels, as detailed in Section 2.6, and calculating vegetation indices from these as well.

#### 2.4. Phenology dates from time series data

We used similar methods to calculate phenology dates from both UAV  $G_{CC}$  and MODIS EVI and  $G_{CC}$ ; these curve fitting methods are described in detail in Klosterman et al. (2014). Briefly, sigmoid functions were fit to vegetation index time series, using a greendown sigmoid (Elmore et al., 2012) for UAV data and a simple sigmoid (Zhang et al., 2003) for MODIS. These curve fit models represent vegetation indices with logistic functions in spring and fall; the greendown sigmoid includes a linear decrease in summer time greenness. Curve fit parameters were estimated using non-linear least squares in Matlab, and phenology dates were calculated from curve fit parameters by finding the dates of extrema in the curvature change rate. We used these methods to calculate dates for the start, middle, and end of canopy development in spring (three spring extrema in CCR), and the middle of senescence in fall (middle of three fall extrema in CCR). An example of derived phenology estimates is shown in Fig. S2. Uncertainties were estimated using the Jacobian matrix of curve fit parameters to approximate the parameter covariance matrix, generate Monte Carlo ensembles of phenology dates, and calculate the variance and inner 95% interval of these ensembles for each phenology date in each grid cell.

Phenology dates from tower-mounted PhenoCams were obtained for the following PhenoCam sites located in or near the study area: “harvard” (image and ROI shown in Fig. S3), “harvardlph”, and “harvardbarn”. PhenoCams had primarily deciduous trees in their ROIs. We used dates calculated from  $G_{CC}$  time series with the generalized sigmoid, a curve fit model with additional flexibility over the greendown sigmoid (Klosterman et al., 2014).

#### 2.5. Ground observations

We used a record of direct observations of leaf phenology for red oak ( $n = 4$  trees), red maple ( $n = 5$ ), yellow birch ( $n = 3$ ), American beech ( $n = 4$ ), and black oak ( $n = 4$ ) made every 3–7 days during spring and fall. Budburst date was calculated as the day when 50% of buds had broken on an individual, and leaf maturity was calculated as the day when at least 50% of the leaves on a tree had reached 75% of

their final size. In autumn, leaf color date was determined as the day when 50% of leaves on a tree had changed color. Linear interpolation was used to infer the progression of budburst, leaf size, and leaf color between observation dates; protocols and data methods are described more fully in Richardson and O’Keefe (2009), and the underlying observational data are available in the Harvard Forest Data Archive (<http://harvardforest.fas.harvard.edu:8080/exist/apps/datasets/showData.html?id=hf003>). The trees under observation, as well as the area of mapped species and the PhenoCam fields of view are shown in Fig. S4 along with the primary study area (MODIS pixel).

Tree species were identified for UAV photography analysis using a map of all woody stems  $\geq 1$  cm diameter at breast height (DBH) within a 35 ha plot (<http://harvardforest.fas.harvard.edu:8080/exist/apps/datasets/showData.html?id=hf253>). The species map included 76% of the study area, with 17,946 woody stems (stems  $\geq 5$  cm DBH shown in Fig. S5). Canopy species composition was calculated as fractional basal area by species of live trees in 10 m grid cells. Grid cells in the wetland had an average of 86 stems and 0.10 m<sup>2</sup> basal area, while those in the forest had an average of 27 stems and 0.43 m<sup>2</sup> basal area. We note that using smaller spatial grids than 10 m increased the chances of incorrectly assigning portions of tree crowns in UAV imagery to grid cells not containing their stems, as we found in separate work that the average length of the major axis of dominant crowns (those most visible in aerial imagery) was 8 m ( $\pm 3$  m standard deviation,  $36 \pm 16$  cm stem DBH,  $n = 30$  trees). We also noted decreased explanatory power of the statistical modeling described below when using smaller grid sizes, another reason we chose 10 m as the finest resolution for analysis.

#### 2.6. Statistical analysis

To examine the correlates of variation in deciduous tree phenology within the primary study area, we performed multiple linear regressions using generalized least squares with the nlme package in the R computing language. As predictors in the regressions, we used a categorical variable to distinguish wetlands and forest, and continuous variables of species composition. We classified grid cells as wetlands or forest based on visual inspection of images, as we observed that the wetlands contained herbaceous vegetation with distinct phenology from trees. We eliminated any 10 m grid cell that had  $< 50\%$  of its area in the images from this analysis. Woody species composition was determined by basal area fraction, using all species that appeared in at least 10 of 372 grid cells within the region of available species data, and had at least 20% basal area fraction in at least one grid cell. The remaining species were lumped into one predictor to ensure the fractional species composition of each grid cell summed to 1. Because species predictors were mixture components, we used a no-intercept regression to eliminate the redundant regression coefficient (Draper and Smith, 1998). Following our observation of spatially autocorrelated residuals in initial results using ordinary least squares regressions, we used generalized least squares to model autocorrelation and obtain more robust coefficient estimates (Dormann et al., 2007).

In order to explore how statistical moments of phenology depend on spatial resolution, we examined various sizes of ROIs of UAV photography by dividing the primary study area. The bottom edge of the study area (250 m MODIS pixel) measured approximately 232 m, and we successively divided this area to get resolutions of 116, 78, ... 10 m. In the larger study area, we used aggregates of Landsat and MODIS pixels: the 48 by 48 set of Landsat pixels was aggregated to obtain resolutions from 30 m through 720 m, and the 8 by 8 set of MODIS pixels for resolutions 250 m through 1 km. MODIS and Landsat pixels were aggregated by first averaging the reflectance values across pixels in each group, then calculating vegetation indices and estimating phenology dates as described above. We aggregated reflectances, as opposed to indices or derived dates, since our goal was to simulate different sensor resolutions. We calculated the standard deviation and skewness of phenology dates for each spatial resolution, and quantified

uncertainty using the 95% confidence interval of 2000 bootstrap samples. We also considered whether the phenology dates of larger, coarser resolution ROIs (25 ROIs, 48 m resolution) in UAV imagery were most closely related to the mean,  $G_{CC}$  amplitude-weighted mean, or median of phenology dates from the smaller, finer resolution ROIs they contained (16 ROIs of 12 m resolution within each of the 25), to determine the transfer function of phenology dates from finer to coarser spatial scales.

### 3. Results

#### 3.1. Landscape phenology

Orthophotos of the study area clearly show leaf-out of deciduous trees (selected dates shown in Fig. 1A–E), with the primary study area becoming greener during the period April–May–June, and deciduous trees becoming harder to distinguish from the evergreens, which were plainly visible on April 30. Senescence reveals differences among deciduous species, with red maples displaying red leaves (Fig. 1D) before red oaks turn a brownish-yellow color (Fig. 1E). The average  $G_{CC}$  of the deciduous community (Fig. 1G) has a larger amplitude of spring time increase than other plant communities, coinciding with the period of leaf-out; evergreen grid cells (classified as  $G_{CC} > 0.39$  before deciduous leaf out, which we found corresponded to approximately 95% evergreen basal area) display a more gradual seasonal progression in  $G_{CC}$  and smaller seasonal amplitude. Wetland areas exhibit relatively independent dynamics, both from each other and from the tree communities, with different amplitudes and timing of greenness changes. Clear differences in phenology among and within plant communities (Fig. 1) are reflected in derived phenophase transition dates (Fig. 2). For example, the wetland areas, in particular wetland 1, greened up later and senesced earlier than the tree communities, as seen both in the  $G_{CC}$  time series and in phenology maps determined from curve fitting (Fig. 2). There is more spatial variation in fall phenology than in spring phenology, both across the primary study area as a whole, and within the deciduous community. Due to the more gradual progression of autumn leaf phenology, the uncertainty of the curve fitting method is larger for fall than spring: two-sided 95% confidence interval widths are

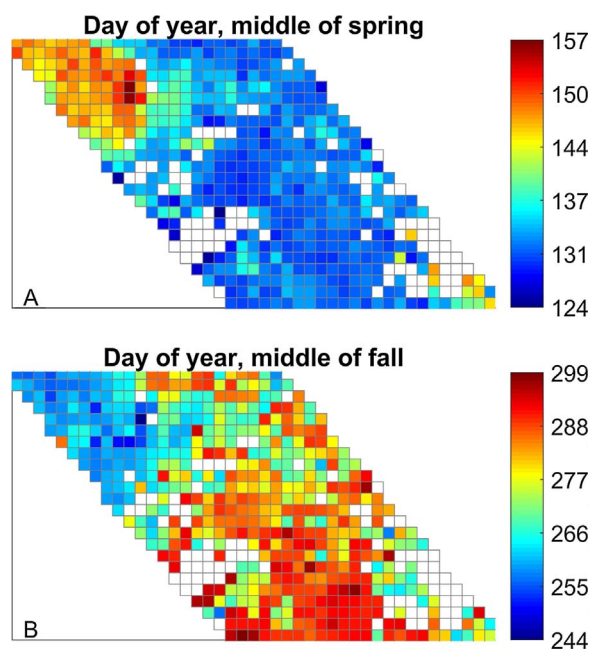


Fig. 2. A, B: Maps of phenology dates for 10 m grid cells in the primary study area, for middle of spring and middle of fall, 2013, determined from curve fitting. Grid cells shown in white failed to generate phenology dates by the curve fitting method, primarily due to lack of  $G_{CC}$  variation in evergreen trees.

11, 7, 14, and 15 days for SOS, MOS, EOS, and MOF, respectively, averaged across all land cover types, and 10, 5, 12, and 14 days within the deciduous land cover type. The transition where the  $G_{CC}$  curve is steepest, the middle of spring, has the lowest average uncertainty. The uncertainties for all seasonal transitions are smaller than the range of dates for that transition (e.g. Fig. 2), indicating UAV photo analysis is effective for exploring phenological differences among communities. In Sections 3.2 and 3.3, we compare start and end of spring to direct observations of phenology because they are closest to bud burst and leaf maturity, but focus on middle of spring for regression analysis (also in Section 3.3) and scaling analyses (Section 3.4), because of greater certainty in this date.

#### 3.2. Differences between and within plant communities

##### 3.2.1. Budburst

Using the land cover classifications shown in Fig. 1F, we explored differences between and within plant communities and validated UAV results with *in situ* observations. The histogram of start of spring dates from UAV imagery (Fig. 3A) has a peak at day of year 124 for the community of all plants. The deciduous trees have the same peak, while the average evergreen date is six days earlier, similar to findings of Richardson et al. (2009), and wetlands four days later (means are different according to *t*-test at 5% significance level). Start of spring dates for the dominant species red oak and red maple match the timing of budburst observations from trees near the study area to within the average inner 95% confidence interval of 10 days for deciduous grid cells. This shows that UAV imagery analysis can reveal statistically significant differences between plant communities' phenology, and provide similar results to ground-based observations at the species level.

PhenoCams located in and near the study area, and MODIS data for the study area and surrounding pixels, provide validation and context for the UAV imagery results. PhenoCams agree with each other on the start of spring to within two days (average DOY 122), and are all within the average 95% confidence interval of the peak of UAV photography dates. The MODIS date for the primary study area (star symbol) is also close to this date, for both MODIS  $G_{CC}$  and MODIS EVI. The means of both the MODIS  $G_{CC}$  and EVI dates for the primary study area and the 8 surrounding pixels are within one day of the mean date of UAV photography ROIs across the community of all plants. Taken together, the similarity with surrounding areas as seen by PhenoCam and MODIS and the relatively small variance of start of spring dates in UAV imagery, in comparison with later transitions (standard deviation 4 days versus 10 days for leaf maturity, Fig. 3B, and 12 days for fall color, Fig. 3C), indicate that most vegetation in the study area begins green-up at roughly the same time. The range between the earliest and latest dates determined from UAV photography (24 days) is however three times that of MODIS (8 days), indicating the presence of finer-scale phenology variability than observable with MODIS.

##### 3.2.2. Leaf maturity

By the end of green-up (Fig. 3B), UAV imagery shows that differences between plant communities become larger: the average date of leaf maturity for evergreens in the primary study area (DOY 151) lags the deciduous leaf maturity date (DOY 141) by over a week, and the corresponding wetland date (DOY 162) is three weeks later (*t*-test at 5% significance level). We note that the PhenoCams, which are focused on the deciduous canopy, all have the same transition date (DOY 139), which is close to the mean deciduous date from UAV photography. However the aggregate phenology of MODIS depends on the index: MODIS  $G_{CC}$  is closer to the deciduous community (mean of 3 by 3 window of MODIS pixels is DOY 142), while EVI is later, and closer to the wetland dates from UAV imagery (mean DOY 150). Deciduous trees in the vicinity of wetland 1 have a later end of spring transition than most other trees (result not shown), a trend already evident during their middle of spring transition (Fig. 2).

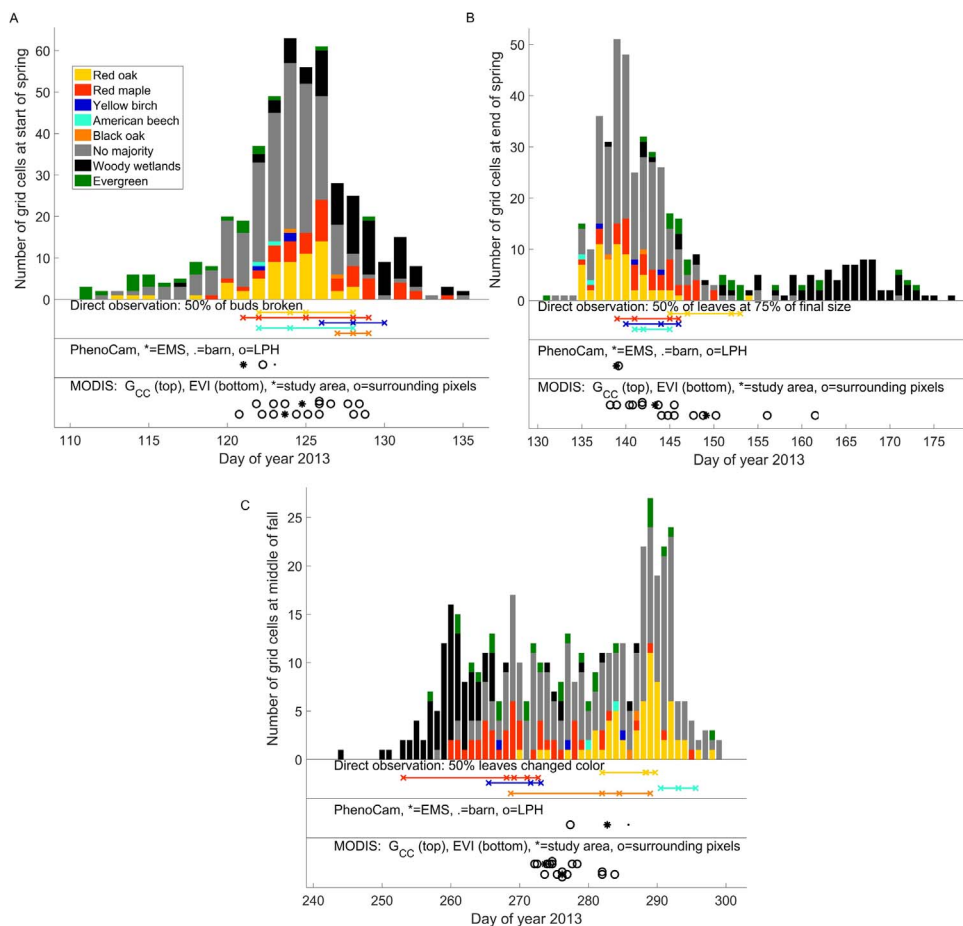


**Fig. 3.** A–C: Histograms of phenology transition dates for each 10 m grid cell (ROI) in UAV imagery for start of spring (bud burst, A), end of spring (leaf maturity, B), and middle of fall (leaf color, C), color coded by plant community type, and in the case of deciduous trees, by species for grid cells with a species majority as determined by basal area fraction (“No majority” indicates grid cells with no majority species, or that were not on the species map). Outliers of more than three standard deviations from the mean have been removed. Below the histograms are shown: ground observations of nearby conifers to dominant species in study area, where the symbols represent individual trees, connected by lines of the same color for each species; PhenoCam transition dates for cameras located in (EMS) and near (barn, LPH) the study area; and MODIS phenology transition dates for the study area and the eight surrounding 250 m MODIS pixels, determined from  $G_{CC}$  and EVI.

### 3.2.3. Autumn leaf color

In fall, differences in the timing of phenology events within the deciduous community are larger than at any point during spring. The difference between average leaf coloring times of red oak and red maple seen in the direct observations (~20 days) is similar to UAV results (Fig. 3C). This indicates that spatial variation of phenology within the deciduous community (Fig. 2B) may be partially explained by spatial differences in species assemblage. Across the deciduous community, the average of UAV photography dates (DOY 281) is close to the average PhenoCam date (DOY 282). However the earlier average of all communities in UAV photography (DOY 277), which appears to be primarily due to the wetlands (average DOY 262), is closer to the MODIS dates for the study area (mean of 3 by 3 window = DOY 275 for  $G_{CC}$ , DOY 278 for EVI). This confirms that MODIS phenology, particularly that of EVI, is similar to that of the community of all plants, while PhenoCams are closer to just the deciduous trees, the land cover type they target, during both spring and autumn transitions.

### 3.3. Biological correlation with landscape variability in phenology and differences between and within deciduous species

We used multiple linear regressions to examine the correlation of phenology dates to biological (species, land cover type) variability across the landscape, and to infer phenology dates of different species. Using semi-variograms to examine spatial autocorrelation of residuals from initial regressions using ordinary least squares, we found that regression residuals were autocorrelated up to a range of 30 m in spring and 150 m in fall, with nuggets of 0.2 and 0.5 respectively (Dormann et al., 2007). Consequently we performed generalized least squares regressions, using these parameters in a spherical autocorrelation model, and report the results here. The generalized least squares

regressions explained 75% of spatial variance in the middle of spring transition, and 56% in the middle of fall transition. Adding the variance of Monte Carlo ensembles over all grid cells, we obtained estimates of curve fitting error, which constituted 7% of phenology variance in spring and 10% in fall (Table S1). Therefore 18% of variance in spring and 34% in fall was due to regression model lack of fit, possibly associated with temperature microclimates or other environmental variability (Fisher et al., 2006), genetic variation within species (Sork et al., 2013), age- or size-related effects (Richardson and O’Keefe, 2009), disturbance, or other factors not included in the model.

The regression coefficients (Table 1) represent inferred phenology dates for the middle of spring and fall transitions of select deciduous species. Wetlands were observed in imagery to have a later spring transition and earlier fall transition than the forest (Figs. 1–3). Similarly, the regression model indicates that the wetlands have a significant ( $p < 0.05$ ) 9-day delay in the middle of spring transition as compared to forested land, and 5-day advance for the middle of fall.

Most deciduous tree species transitioned through middle of spring within a week of each other, while in fall the earlier dominant species (yellow birch, red maple) senesced roughly two to three weeks earlier than the later ones (red oak, American beech). Species abundance is reflected in the certainty with which transition dates could be determined: the species in Table 1 are ordered by total basal area, and the most prevalent species near the top of the list have smaller standard errors than the rarer species.

We compared species transition dates from UAV photography analysis with a ground truth of direct observations, calculating a similar regression to that reported in Table 1 for middle of spring, but with start of spring to compare with budburst observations, and using the autumn results from Table 1 in comparison with leaf color observations. We found that in spring, the regression analysis resulted in phenology dates

**Table 1**

Regression coefficients and standard errors (SE) for the multiple linear regression of middle of spring and fall dates of grid cells (N = 372). Predictors include a categorical variable for wetland land cover type (as opposed to forest) and species composition by basal area fraction for the indicated species (select deciduous species). Species are ordered by prevalence in terms of total basal area in all grid cells, and include red oak (*Quercus rubra*), red maple (*Acer rubrum*), yellow birch (*Betula alleghaniensis*), American beech (*Fagus grandifolia*), black oak (*Quercus velutina*), black cherry (*Prunus serotina*), winterberry (*Ilex verticillata*), white ash (*Fraxinus americana*), black birch (*Betula lenta*), paper birch (*Betula papyrifera*), highbush blueberry (*Vaccinium corymbosum*), uncertain birches in the genus *Betula*, and maleberry (*Lyonia ligustrina*).

Variable	Spring Coefficient	Spring SE	Fall Coefficient	Fall SE
Cover type wetland	9	0.8	-5	2.4
Red oak	132	0.5	289	2.7
Red maple	134	0.5	272	2.7
Yellow birch	131	1.4	273	4.5
American beech	132	1.5	290	4.6
Black oak	134	2.3	292	6.1
Black cherry	132	4.3	272	12.2
Winterberry	138	1.3	273	4.4
White ash	134	5.1	255	14.8
Black birch	129	3.2	283	9.3
Paper birch	131	3.4	268	10.2
Highbush blueberry	135	3.7	262	10.7
Other birch	135	2.6	278	7.8
Maleberry	136	3.9	268	11.5

within the range of observed trees for most species (Fig. 4A). Autumn regression results were also close to observations of leaf color (Fig. 4B), with oaks and beeches roughly two to three weeks later than maples and birches from both methods. For the most populous species (red oak and red maple), the range between the earliest and latest individuals under direct observation was larger than the regression confidence intervals in spring. This indicates that the more thorough sampling of dominant species allowed by UAV photography can lead to more precise characterization of species-level phenology transition dates than direct observation of a small number of individuals (3–5 per species). However we note that in autumn, most species were more precisely characterized by direct observation, likely corresponding to the fact that species and land cover explain less phenological variability in fall (56%) than in spring (75%). To examine within-species variability, we isolated 10 m grid cells that had more than 75% of one tree species by basal area in UAV imagery; these dominant species are red oak and red maple. We found more variance in middle of fall than start of spring dates for these species, and more variance for red maple than red oak in fall (Table 2). Similar results were found for the same species under direct observation. The larger variance of red maple in autumn may be due to its spatial distribution: red maple is relatively evenly spread throughout the study area, both in and around wetland areas, as well as in upland areas, and therefore inhabits a wider range of land cover types than red oak, which tends to be absent from wetter areas (Fig. S5). Across New England, red maples growing in and around wetland areas tend to change color well in advance of those on better-drained soils. These results indicate that within-species variation, which may account for 18% of landscape phenology variation in spring and 34% in fall, could be unevenly distributed among species.

3.4. Scaling of phenology

In our scaling analysis, we used UAV photography to explore phenophase transitions within Landsat and MODIS pixels, and link observations at different scales. First, we examined the statistical properties of transition dates at different spatial resolutions across these imaging platforms. The goals of this analysis were to see whether and how patterns in statistical moments from the coarser scales of remote sensing extended to the higher resolution available with UAV photography, and how much variation in phenology occurred at finer scales than satellite remote sensing.

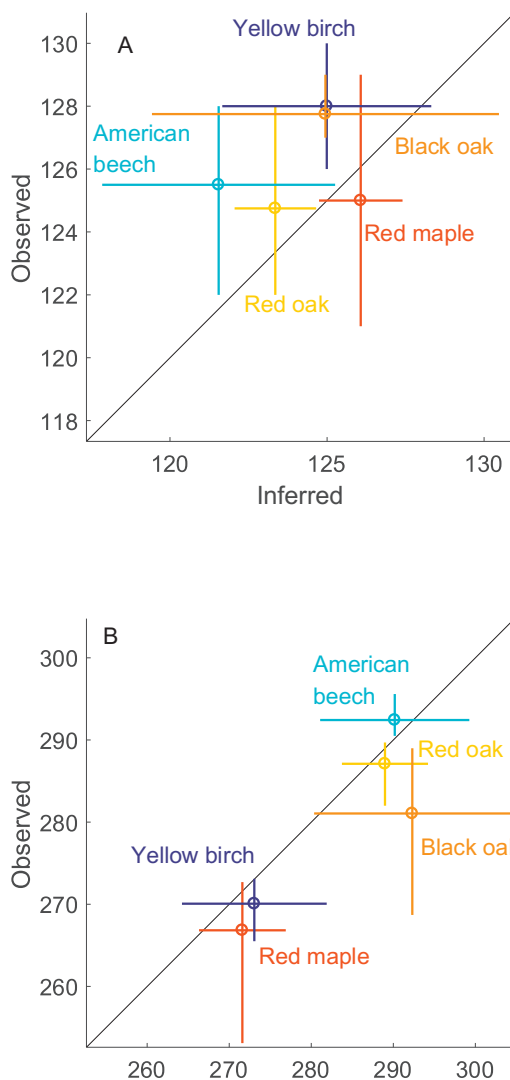


Fig. 4. A, B: Comparison of start of spring (50% budburst) dates and middle of fall (50% leaf color) dates inferred from linear regression analysis with species averages from direct observation of trees, for species with a majority of basal area in at least one 10 m grid cell. The diagonal line is the one–one line; horizontal lines are the 95% confidence intervals of inferred dates; vertical lines are the ranges between earliest and latest trees under observation.

**Table 2**

Comparison of within-species variability in UAV photography and direct observation: standard deviations (SD) of start of spring (budburst) dates and middle of fall (50% leaf color) dates. Grid cells are those with greater than 75% basal area of the indicated species.

Species	N grid cells	Start of spring SD	Middle of fall SD	N trees under direct observation	Budburst SD	Leaf color SD
Red oak	20	3.4	3.6	4	2.5	3.5
Red maple	42	3.0	8.5	5	3.5	7.9

Overall, we found that spatial variability in phenology declines as spatial resolution becomes coarser. Using ROIs ranging from 10 m to 1 km, standard deviation of phenological transition dates decreases with increasing pixel size, following a significant ( $p < 0.001$ ) linear trend with logarithm of pixel length across observation platforms (UAV, Landsat, and MODIS EVI, with similar results, not shown, from MODIS  $G_{CC}$ ) in both middle of spring and middle of fall (Fig. 5A, B). While there is an apparent discontinuity between UAV and Landsat standard deviations in spring, and to a lesser extent in fall, this is probably

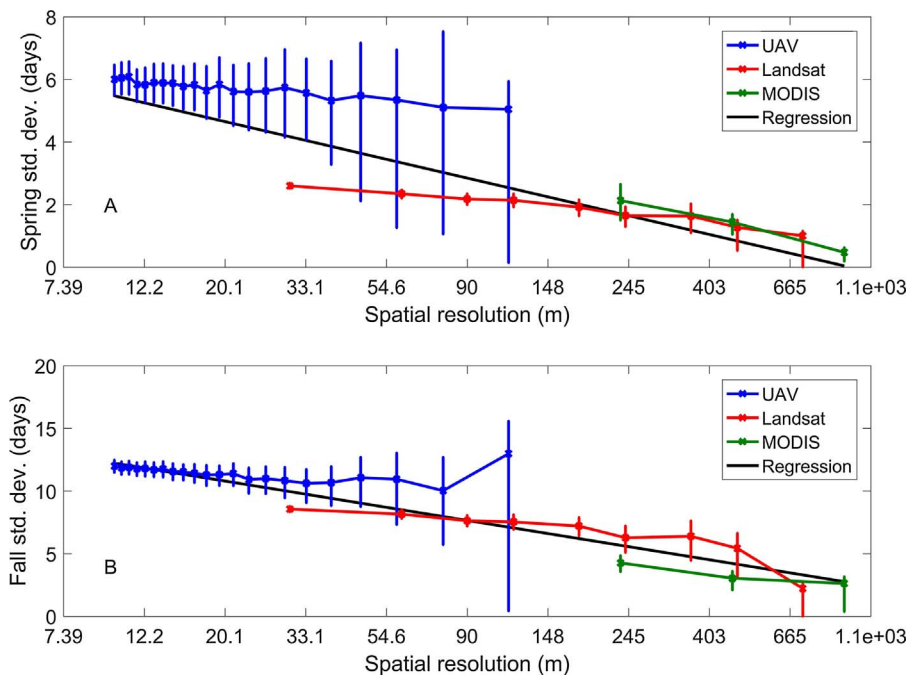


Fig. 5. A, B: Relation between standard deviation of phenology dates (middle of spring and fall) and spatial resolution in pixel size (m). Vertical bars indicate 95% confidence intervals from bootstrap sampling, and the black line is a regression using all the data, weighted by the inverse of confidence interval width. Spring linear regression: slope =  $-1.2$ ,  $R^2 = 0.76$ ,  $p < 0.001$ . Fall linear regression: slope =  $-2.1$ ,  $R^2 = 0.90$ ,  $p < 0.001$ .

caused by the area of later spring (earlier fall) phenology in the wetlands (Fig. 2), that constitutes a substantial fraction of the UAV study area. The bootstrap samples used to generate confidence intervals may not include this area, particularly at larger UAV pixel sizes, resulting in lower variance for some samples; this is reflected in the low end of the 95% confidence intervals for these pixel sizes, which are close to Landsat. We also tried sampling only the non-wetland regions of the UAV study area and found a more clearly decreasing trend in spatial variance with increasing pixel size. Because the wetlands had later spring phenology than the forest, the distribution of spring dates in the UAV study area was skewed toward later dates (skewness results not shown).

However the larger study area as viewed by Landsat and MODIS had a skew close to zero for spring, and both areas did for fall, indicating that across the landscape at Harvard Forest, localized regions of later phenology, such as the wetlands in the primary study area, are as common as those of earlier phenology. These results imply that if we had UAV photography over the larger study area observed with Landsat and MODIS, we would likely observe a smooth transition in variance across all observation platforms.

Standard deviation declines to near zero for both seasons at the largest pixel sizes, indicating remote sensing at a resolution of roughly 1 km combines organisms and landscapes to such an extent that little spatial variation is observed. Importantly, we note that most of the spatial variability in phenology at Harvard Forest occurs at finer scales than observable with MODIS.

In the second part of our scaling analysis, we examined the transfer function governing the representation of finer scale phenology within larger pixel sizes, using UAV photography at  $\sim 12$  m and  $\sim 48$  m resolutions. We found that dates of larger pixels were most closely related to the median dates of their constituent smaller pixels in fall, while in spring the median was similar to the mean and  $G_{CC}$  amplitude-weighted mean (Table 3).

#### 4. Discussion

##### 4.1. Patterns in community phenology

Using a combination of UAV photography and remote sensing (MODIS NBAR and Landsat), we explore how the diverse phenological

Table 3

RMSEs (days) of the comparison between  $\sim 48$  m pixels and summary statistics of the 16–12 m pixels they contain ( $n = 23$ , out of an attempted 25. Dates could not be estimated for all grid cells as shown in Fig. 2).

Statistic	Spring RMSE	Fall RMSE
Mean	0.6	3.6
$G_{CC}$ amplitude-weighted mean	0.5	3.2
Median	0.7	2.1

behaviors of different plant communities aggregate to produce an ecosystem-level phenology. We find that this scaling depends on which seasonal transition is under consideration. Because plants from all communities start to develop foliage around the same time, the distribution of phenology dates from UAV photography has a clear peak at the start of spring, and a small standard deviation (4 days). The MODIS  $G_{CC}$  and EVI dates are very close to this, for the UAV photography area as well as surrounding MODIS pixels (Fig. 3A). However at the end of spring, plants have more diverse phenology (standard deviation 10 days) and the wetland community lags the others by approximately two weeks. MODIS  $G_{CC}$  and EVI phenology of the study area are both within 3 days of the mean phenology of all communities from UAV photography at the end of spring. However while MODIS  $G_{CC}$  is also close to the mean of deciduous grid cells (2 days difference), MODIS EVI is 8 days later. This is a key point since MODIS EVI is often assumed to represent deciduous trees in modeling of mixed forest ecosystem function (e.g. Medvigy et al., 2009). In terms of carbon uptake, a phenological bias of a week later spring transition corresponds to a substantial decrease in net ecosystem productivity of approximately 28 g C per  $m^2$  (Richardson et al., 2010).

Our results show that UAV photography is an effective tool for understanding how divergent phenological behaviors of plant communities relate to aggregate landscape phenology. We also note that UAV imagery provides a more accurate representation of heterogeneous landscape phenology around point measurements of ecosystem-scale processes (e.g. carbon fluxes) than tower-mounted instruments such as PhenoCams. This information could be useful for calibrating models and interpreting measurements of ecological processes that depend on plant phenology, such as canopy scale photosynthesis.

#### 4.2. Biological components of landscape variation

By combining UAV photography with a detailed species map and land cover classification, we examine the biological correlates of fine-scale variance in landscape phenology. We find that species composition and land cover explain most of the spatial variance in phenology in spring (75%) and fall (56%). These results provide a spatially extensive validation indicating that the practice of upscaling phenology based on relative species abundance, an approach already used by some researchers (Liang et al., 2011), accounts for the dominant factor in phenological variability within deciduous forest communities.

From this analysis we also infer species-specific phenophase transition dates, and reference them to *in situ* observations of leaf phenology events. Within the deciduous community, bud burst and leaf maturity match the start and end of spring metrics from UAV photography, respectively, while the colors of fall senescence reach their halfway point at approximately the same time as the middle of fall dates calculated from UAV photography (Fig. 3A–C). These findings are similar to an earlier comparison of direct observations and transition dates derived from tower-mounted PhenoCams (Keenan et al., 2014a), as well as a recent study on budburst observations in comparison to  $G_{CC}$  from UAV photography (Berra et al., 2016). We also find a similar order of species phenology events to a previous study at Harvard Forest (Richardson and O’Keefe, 2009). Within species, we see that the nominal variability of deciduous tree phenology observed in UAV photography is similar to that revealed by direct observation (Table 2). However by accounting for land cover and species fractions on a 10 m grid, in most cases we are able to infer phenology dates of dominant species with more certainty than from direct observation (Fig. 4A, B). This analysis demonstrates the statistical power that can be gained from integrating the large spatial coverage of UAV photography with species data on a fine spatial scale.

#### 4.3. Scaling from organisms to the landscape

Remote sensing is an essential research tool for global phenology monitoring. However remote sensing platforms generally face a tradeoff where increased spatial resolution is associated with decreased temporal resolution. In phenology studies, high spatial resolution is needed to see differences between communities in heterogeneous ecosystems such as mixed forests, while temporal resolution must be sufficient to accurately capture rapid phenological changes such as budburst (Pfeifer et al., 2012). Methods have been developed to leverage multi-year records of high spatial resolution (*i.e.* 30 m) remote sensing at a temporal resolution of weekly or longer, using annual deviations from the long term mean (Melaas et al., 2013). However the combination of high temporal (*i.e.* daily), low spatial (250 m or larger) resolution is needed for reliable yearly satellite observations during times of phenological change (Schaaf et al., 2002, 2011; Shuai et al., 2013; Verger et al., 2016). This is because in some years, clouds may prevent weekly satellite observations from imaging the earth’s surface during the entire period of leaf-out, as we found with Landsat at Harvard Forest in 2013. Since different resolutions of satellite remote sensing are useful for different phenology research questions, it is important to know how phenological information transfers across scales. We explore the mathematical nature of this scaling process with UAV imagery.

Scaling laws are fundamental to ecology, starting with the species-area relationship (Arrhenius, 1921). They receive continued attention as spatial data from remote sensing become increasingly available (Woodcock and Strahler, 1987). In the context of plant canopies, investigators have examined how ecological processes scale at an instant in time, to give general guidance in statistical methods for translating fine scale information to coarser scales (Rastetter et al., 1992), and to determine the effect of preserving different statistical moments in the upscaling process (Stoy et al., 2009). Spatial scaling of the temporal aspect of canopy phenology has received relatively less attention.

We analyze the scaling of phenology transition dates at resolutions from 10 m to 1 km, and find a linear relationship between logarithm of pixel size and standard deviation in phenology transition dates (Fig. 5A, B). These results are similar to the scaling of time-invariant snapshots of ecological observations, such as the species-area law and the scaling of canopy status as measured by the normalized difference vegetation index (NDVI) (Stoy et al., 2009). Our findings indicate that significant variability is lost in the transition to coarse scale observations. Since most of the variability we observe in phenology is at finer scales than the larger pixel sizes of remote sensing (Fig. 5A, B), our results suggest that accurate models of ecosystem-scale phenology should consider finer scale phenology variability than available from MODIS.

We also explore the statistical nature of the transfer from phenology dates at fine spatial resolution to the dates of larger regions, using two pixel sizes to analyze UAV photography (400 grid cells at ~12 m resolution, aggregating to 25 grid cells at ~48 m resolution). We find that in the relatively quick spring transition, phenology scales with the mean, similar to results from a previous study that fused Landsat and MODIS observations (Fisher and Mustard, 2007), and in agreement with a community- and area-weighted mean upscaling approach using individual tree observations (Liang et al., 2011). Our results advance these studies by showing the same pattern in whole-ecosystem observations of all plants visible in UAV photography, at a spatial resolution on the scale of dominant tree crowns.

We also note that the median and  $G_{CC}$  amplitude-weighted mean describe upscaling with essentially the same accuracy as the mean in spring. In the more gradual fall transition however, greater spatial variance in phenology led to larger differences between scaling methods. Here we found that the median of finer resolution dates was closer to the coarser scale date than these other statistics. The amplitude-weighted mean places more emphasis on areas with larger seasonal change in  $G_{CC}$ , which are likely to be “more deciduous” than areas with smaller amplitude. Our results indicate that for autumn phenology in our study area at Harvard Forest, transition dates at a coarser spatial scale are not especially influenced by small areas that have greater seasonal changes in greenness, or by particularly early or late transitions that would affect the mean. These results advance the mathematical understanding of how the phenology of larger pixel sizes relates to the phenology of smaller pixels contained therein.

## 5. Conclusion

Understanding phenology’s role in earth system processes now and in the future depends on accurate characterization of plants, as they function at scales from the individual to the landscape. Going from plants and forest stands, where phenology is most tangible to us as observers, to the ecosystems which global observations and models use, requires a quantitative understanding of how phenology scales (Potter et al., 2013). To serve this need, we presented here the first observation of forest phenology at the ecosystem scale, with spatial resolution on the order of individuals, and found that three levels of organization could be used to describe phenology at our study site:

- Diverse plant communities, such as wetlands, evergreens, and deciduous trees
- Species diversity within communities
- Within-species variance, possibly due to microenvironments, genetic variation, disturbance, or tree age

We combined coarse (250 m MODIS) and intermediate (30 m Landsat) resolution remote sensing with UAV photography (10 m resolution) to examine the statistical features of scaling in phenology. From this we found that the spatial standard deviation of phenophase transition dates across the landscape increases in a linear fashion with the logarithm of smaller pixel size. Most of the variability that can be gained from observing smaller pixels occurs at finer scales than MODIS.

Using a detailed species map, we determined that species and land cover variability correlate with most of the fine-scale variance of phenology in spring (75%) and fall (56%). Our results suggest that using a species- and community-based scaling approach to modeling ecosystem phenology would account for the dominant factors in spatial variability.

We demonstrate the potential of the large spatial coverage and fine spatial and temporal resolutions of UAV photography for obtaining phenology observations that could be used to validate ecosystem models, and to interpret integrated measurements of heterogeneous ecosystem processes like canopy photosynthesis. As UAV technology continues to improve and become less costly, we advocate for wider use of UAVs in phenology studies, to address research objectives that would benefit from increased access to aerial survey data.

## Funding

The authors gratefully acknowledge several funding sources. Stephen was supported by NASA Headquarters under the NASA Earth and Space Science Fellowship Program – Grant 14-EARTH14R-23. Jon was supported by a National Science Foundation Graduate Research Fellowship under Grant No. DGE-1247312. Arturo Martinez and Sidni Frederick were supported by the Harvard Forest Summer Research Program in Forest Ecology through grants from the National Science Foundation's Research Experiences for Undergraduates program (award DBI-1003938) and NASA's Global Climate Change Education program. The PhenoCam project has been supported by the Northeastern States Research Cooperative, NSF's Macrosystems Biology program (awards EF-1065029 and EF-1702697), DOE's Regional and Global Climate Modeling program (award DE-SC0016011), and the US National Park Service Inventory and Monitoring Program and the USA National Phenology Network (grant number G10AP00129 from the United States Geological Survey). Additional support was received from the National Science Foundation under the Harvard Forest Long-Term Ecological Research Program (NSF DEB-1237491), the Harvard Center for Geographic Analysis, and NASA grants NNX14AI73G and NNX14AD57G. Funding sources had no involvement in study design, collection, analysis or interpretation of data, writing of the report, or the decision to submit the article for publication.

## Acknowledgements

We would like to thank the woods crew and all at Harvard Forest for their enthusiastic support and assistance, as well as Michael Toomey, Jonathan Dandois, Stephen Gienow, Erle Ellis and the Ecosynth project for invaluable help and guidance. We also thank two anonymous reviewers for their helpful comments, which resulted in many improvements to the manuscript.

## Appendix A. Supplementary data

Supplementary data associated with this article can be found, in the online version, at <http://dx.doi.org/10.1016/j.agrformet.2017.10.015>.

## References

Ahrens, H.E., Bruegger, R., Stoeckli, R., Schenk, J., Michna, P., Jeanneret, F., Wanner, H., Eugster, W., 2008. Quantitative phenological observations of a mixed beech forest in northern Switzerland with digital photography. *J. Geophys. Res.* 113, G04004. <http://dx.doi.org/10.1029/2007jg000650>.

Anderson, K., Gaston, K.J., 2013. Lightweight unmanned aerial vehicles will revolutionize spatial ecology. *Front. Ecol. Environ.* 11, 138–146. <http://dx.doi.org/10.1890/120150>.

Arrhenius, O., 1921. Species and area. *J. Ecol.* 9, 95–99.

Ault, T.R., Schwartz, M.D., Zurita-Milla, R., Weltzin, J.F., Betancourt, J.L., 2015. Trends and natural variability of spring onset in the coterminous United States as evaluated by a new gridded dataset of spring indices. *J. Clim.* 28, 8363–8378. <http://dx.doi.org/10.1175/JCLI-D-14-00736.1>.

Badeck, F.-W., Bondeau, A., Bottcher, K., Doktor, D., Lucht, W., Schaber, J., Sitch, S., 2004. Responses of spring phenology to climate change. *New Phytol.* 162, 295–309. <http://dx.doi.org/10.1111/j.1469-8137.2004.01059.x>.

Berra, E.F., Gaulton, R., Barr, S., 2016. Use of a digital camera onboard a UAV to monitor spring phenology at individual tree level. In: 2016 IEEE International Geoscience and Remote Sensing Symposium (IGARSS). IEEE. pp. 3496–3499. <http://dx.doi.org/10.1109/IGARSS.2016.7729904>.

Brown, T.B., Hultine, K.R., Steltzer, H., Denny, E.G., Denslow, M.W., Granados, J., Henderson, S., Moore, D., Nagai, S., SanClements, M., Sánchez-Azofeifa, A., Sonnentag, O., Tazik, D., Richardson, A.D., 2016. Using phenocams to monitor our changing earth: toward a global phenocam network. *Front. Ecol. Environ.* 14, 84–93. <http://dx.doi.org/10.1002/fee.1222>.

Campagnolo, M.L., Sun, Q., Liu, Y., Schaaf, C., Wang, Z., Román, M.O., 2016. Estimating the effective spatial resolution of the operational BRDF, albedo, and nadir reflectance products from MODIS and VIIRS. *Remote Sens. Environ.* 175, 52–64. <http://dx.doi.org/10.1016/j.rse.2015.12.033>.

Cleland, E.E., Chuine, I., Menzel, A., Mooney, H.A., Schwartz, M.D., 2007. Shifting plant phenology in response to global change. *Trends Ecol. Evol.* 22, 357–365. <http://dx.doi.org/10.1016/j.tree.2007.04.003>.

Dandois, J.P., Ellis, E.C., 2013. High spatial resolution three-dimensional mapping of vegetation spectral dynamics using computer vision. *Remote Sens. Environ.* 136, 259–276. <http://dx.doi.org/10.1016/j.rse.2013.04.005>.

Doktor, D., Bondeau, A., Koslowski, D., Badeck, F.-W., 2009. Influence of heterogeneous landscapes on computed green-up dates based on daily AVHRR NDVI observations. *Remote Sens. Environ.* 113, 2618–2632. <http://dx.doi.org/10.1016/j.rse.2009.07.020>.

Dormann, C.F., McPherson, J.M., Araújo, M.B., Bivand, R., Bolliger, J., Carl, G.G., Davies, R., Hirzel, A., Jetz, W., Daniel Kissling, W., Kühn, I., Ohlemüller, R.R., Peres-Neto, P., Reineking, B., Schröder, B.M., Schurr, F., Wilson, R., 2007. Methods to account for spatial autocorrelation in the analysis of species distributional data: a review. *Ecography (Cop.)* 30, 609–628. <http://dx.doi.org/10.1111/j.2007.0906-7590.05171.x>.

Dragoni, D., Schmid, H.P., Wayson, C.A., Potter, H., Grimmond, C.S.B., Randolph, J.C., 2011. Evidence of increased net ecosystem productivity associated with a longer vegetated season in a deciduous forest in south-central Indiana, USA. *Glob. Change Biol.* 17, 886–897. <http://dx.doi.org/10.1111/j.1365-2486.2010.02281.x>.

Draper, N.R., Smith, H., 1998. *Applied Regression Analysis*, 3rd ed. John Wiley & Sons, New York.

Elmore, A.J., Guinn, S.M., Minsley, B.J., Richardson, A.D., 2012. Landscape controls on the timing of spring, autumn, and growing season length in mid-Atlantic forests. *Glob. Change Biol.* 18, 656–674. <http://dx.doi.org/10.1111/j.1365-2486.2011.02521.x>.

Fisher, J.I., Mustard, J.F., 2007. Cross-scalar satellite phenology from ground, Landsat, and MODIS data. *Remote Sens. Environ.* 109, 261–273. <http://dx.doi.org/10.1016/j.rse.2007.01.004>.

Fisher, J., Mustard, J., Vadeboncoeur, M., 2006. Green leaf phenology at Landsat resolution: scaling from the field to the satellite. *Remote Sens. Environ.* 100, 265–279. <http://dx.doi.org/10.1016/j.rse.2005.10.022>.

Gatzliolis, D., Lienard, J.F., Vogs, A., Strigul, N.S., 2015. 3D tree dimensionality assessment using photogrammetry and small unmanned aerial vehicles. *PLoS One* 10, e0137765. <http://dx.doi.org/10.1371/journal.pone.0137765>.

Huete, A., Didan, K., Miura, T., Rodriguez, E.P., Gao, X., Ferreira, L.G., 2002. Overview of the radiometric and biophysical performance of the MODIS vegetation indices. *Remote Sens. Environ.* 83, 195–213. [http://dx.doi.org/10.1016/S0034-4257\(02\)00096-2](http://dx.doi.org/10.1016/S0034-4257(02)00096-2).

Hufkens, K., Friedl, M., Sonnentag, O., Braswell, B.H., Milliman, T., Richardson, A.D., 2012. Linking near-surface and satellite remote sensing measurements of deciduous broadleaf forest phenology. *Remote Sens. Environ.* 117, 307–321. <http://dx.doi.org/10.1016/j.rse.2011.10.006>.

Ibáñez, I., Primack, R.B., Miller-Rushing, A.J., Ellwood, E., Higuchi, H., Lee, S.D., Kobori, H., Silander, J.A., 2010. Forecasting phenology under global warming. *Philos. Trans. R. Soc. Lond. B: Biol. Sci.* 365, 3247–3260. <http://dx.doi.org/10.1098/rstb.2010.0120>.

Jarvis, P.G., 1995. Scaling processes and problems. *Plant Cell Environ.* 18, 1079–1089. <http://dx.doi.org/10.1111/j.1365-3040.1995.tb00620.x>.

Keenan, T.F., Darby, B., Felts, E., Sonnentag, O., Friedl, M.A., Hufkens, K., O'Keefe, J., Klosterman, S., Munger, J.W., Toomey, M., Richardson, A.D., 2014a. Tracking forest phenology and seasonal physiology using digital repeat photography: a critical assessment. *Ecol. Appl.* 24, 1478–1489. <http://dx.doi.org/10.1890/1365-2745.2013.0652.1>.

Keenan, T.F., Gray, J., Friedl, M.A., Toomey, M., Bohrer, G., Hollinger, D.Y., Munger, J.W., O'Keefe, J., Schmid, H.P., Wing, I.S., Yang, B., Richardson, A.D., 2014b. Net carbon uptake has increased through warming-induced changes in temperate forest phenology. *Nat. Clim. Change* 4, 598–604. <http://dx.doi.org/10.1038/nclimate2253>.

Klosterman, S.T., Hufkens, K., Gray, J.M., Melaes, E., Sonnentag, O., Lavine, I., Mitchell, L., Norman, R., Friedl, M.A., Richardson, A.D., 2014. Evaluating remote sensing of deciduous forest phenology at multiple spatial scales using PhenoCam imagery. *Biogeosciences* 11. <http://dx.doi.org/10.5194/bg-11-4305-2014>.

Liang, L., Schwartz, M.D., Fei, S., 2011. Validating satellite phenology through intensive ground observation and landscape scaling in a mixed seasonal forest. *Remote Sens. Environ.* 115, 143–157. <http://dx.doi.org/10.1016/j.rse.2010.08.013>.

Lisein, J., Michez, A., Claessens, H., Lejeune, P., 2015. Discrimination of deciduous tree species from time series of unmanned aerial system imagery. *PLoS One* 10, e0141006. <http://dx.doi.org/10.1371/journal.pone.0141006>.

Lucier, A., Turner, D., King, D.H., Robinson, S.A., 2014. Using an Unmanned Aerial Vehicle (UAV) to capture micro-topography of Antarctic moss beds. *Int. J. Appl. Earth Obs. Geoinf.* 27, 53–62. <http://dx.doi.org/10.1016/j.jag.2013.05.011>.

Medvigy, D., Wofsy, S.C., Munger, J.W., Hollinger, D.Y., Moorcroft, P.R., 2009. Mechanistic scaling of ecosystem function and dynamics in space and time:

- ecosystem demography model version 2. *J. Geophys. Res.* 114, G01002. <http://dx.doi.org/10.1029/2008JG000812>.
- Melaas, E.K., Friedl, M.A., Zhu, Z., 2013. Detecting interannual variation in deciduous broadleaf forest phenology using Landsat TM/ETM+ data. *Remote Sens. Environ.* 132, 176–185. <http://dx.doi.org/10.1016/j.rse.2013.01.011>.
- Menzel, A., Sparks, T.H., Estrella, N., Koch, E., Aasa, A., Ahas, R., Alm-Kübler, K., Bissolli, P., Braslavská, O., Briede, A., Chmielewski, F.M., Crepinsek, Z., Curnel, Y., Dahl, Å., Defila, C., Donnelly, A., Filella, Y., Jatczak, K., Måge, F., Mestre, A., Nordli, Ø., Peñuelas, J., Pirinen, P., Remišová, V., Scheffinger, H., Striz, M., Susnik, A., Van Vliet, A.J.H., Wielgolaski, F.-E., Zach, S., Züst, A., 2006. European phenological response to climate change matches the warming pattern. *Glob. Change Biol.* 12, 1969–1976. <http://dx.doi.org/10.1111/j.1365-2486.2006.01193.x>.
- Miller-Rushing, A., Primack, R., 2008. Global warming and flowering times in Thoreau's Concord: a community perspective. *Ecology* 89, 332–341. <http://dx.doi.org/10.1890/07-0068.1>.
- Morisette, J.T., Richardson, A.D., Knapp, A.K., Fisher, J.I., Graham, E.A., Abatzoglou, J., Wilson, B.E., Breshears, D.D., Henebry, G.M., Hanes, J.M., Liang, L., 2009. Tracking the rhythm of the seasons in the face of global change: phenological research in the 21st century. *Front. Ecol. Environ.* 7, 253–260. <http://dx.doi.org/10.1890/070217>.
- Pfeifer, M., Disney, M., Quaipe, T., Marchant, R., 2012. Terrestrial ecosystems from space: a review of earth observation products for macroecology applications. *Glob. Ecol. Biogeogr.* 21, 603–624. <http://dx.doi.org/10.1111/j.1466-8238.2011.00712.x>.
- Polgar, C.A., Primack, R.B., 2011. Leaf-out phenology of temperate woody plants: from trees to ecosystems. *New Phytol.* 191, 926–941. <http://dx.doi.org/10.1111/j.1469-8137.2011.03803.x>.
- Potter, K.A., Arthur Woods, H., Pincebourde, S., 2013. Microclimatic challenges in global change biology. *Glob. Change Biol.* 19, 2932–2939. <http://dx.doi.org/10.1111/gcb.12257>.
- Rastetter, E.B., King, A.W., Cosby, B.J., Hornberger, G.M., O'Neill, R.V., Hobbie, J.E., 1992. Aggregating fine-scale ecological knowledge to model coarser-scale attributes of ecosystems. *Ecol. Appl.* 2, 55–70. <http://dx.doi.org/10.2307/1941889>.
- Richardson, A.D., O'Keefe, J., 2009. Phenological differences between understory and overstory. In: Noormets, A. (Ed.), *Phenology of Ecosystem Processes*. Springer, pp. 87–117.
- Richardson, A.D., Jenkins, J.P., Braswell, B.H., Hollinger, D.Y., Ollinger, S.V., Smith, M.-L., 2007. Use of digital webcam images to track spring green-up in a deciduous broadleaf forest. *Oecologia* 152, 323–334. <http://dx.doi.org/10.1007/s00442-006-0657-z>.
- Richardson, A.D., Braswell, B.H., Hollinger, D.Y., Jenkins, J.P., Ollinger, S.V., 2009. Near-surface remote sensing of spatial and temporal variation in canopy phenology. *Ecol. Appl.* 19, 1417–1428. <http://dx.doi.org/10.1890/08-2022.1>.
- Richardson, A.D., Black, T.A., Ciais, P., Delbart, N., Friedl, M.A., Gobron, N., Hollinger, D.Y., Kutsch, W.L., Longdoz, B., Luyssaert, S., Migliavacca, M., Montagnani, L., Munger, J.W., Moors, E., Piao, S., Rebmann, C., Reichstein, M., Saigusa, N., Tomelleri, E., Vargas, R., Varlagin, A., 2010. Influence of spring and autumn phenological transitions on forest ecosystem productivity. *Philos. Trans. R. Soc. Lond. B: Biol. Sci.* 365, 3227–3246. <http://dx.doi.org/10.1098/rstb.2010.0102>.
- Richardson, A.D., Keenan, T.F., Migliavacca, M., Ryu, Y., Sonnentag, O., Toomey, M., 2013. Climate change, phenology, and phenological control of vegetation feedbacks to the climate system. *Agric. For. Meteorol.* 169, 156–173. <http://dx.doi.org/10.1016/j.agrformet.2012.09.012>.
- Schaaf, C.B., Gao, F., Strahler, A.H., Lucht, W., Li, X., Tsang, T., Strugnell, N.C., Zhang, X., Jin, Y., Muller, J.-P., Lewis, P., Barnsley, M., Hobson, P., Disney, M., Roberts, G., Dunderdale, M., Doll, C., d'Entremont, R.P., Hu, B., Liang, S., Privette, J.L., Roy, D., 2002. First operational BRDF, albedo nadir reflectance products from MODIS. *Remote Sens. Environ.* 83, 135–148. [http://dx.doi.org/10.1016/S0034-4257\(02\)00091-3](http://dx.doi.org/10.1016/S0034-4257(02)00091-3).
- Schaaf, C., Martonchik, J., Pinty, B., Govaerts, Y., Gao, F., Lattanzio, A., Liu, J., Strahler, A., Taberner, M., 2008. Retrieval of Surface albedo from satellite sensors. *Advances in Land Remote Sensing*. Springer, Netherlands, Dordrecht, pp. 219–243. [http://dx.doi.org/10.1007/978-1-4020-6450-0\\_9](http://dx.doi.org/10.1007/978-1-4020-6450-0_9).
- Schaaf, C.L.B., Liu, J., Gao, F., Strahler, A.H., 2011. MODIS albedo and reflectance anisotropy products from aqua and terra. In: In: Ramachandran, B., Justice, C., Abrams, M. (Eds.), *Land Remote Sensing and Global Environmental Change: NASA's Earth Observing System and the Science of ASTER and MODIS, Remote Sensing and Digital Image Processing Series*, vol. 11 Springer-Verlag p. 873.
- Schwartz, M.D., Ahas, R., Aasa, A., 2006. Onset of spring starting earlier across the Northern Hemisphere. *Glob. Change Biol.* 12, 343–351. <http://dx.doi.org/10.1111/j.1365-2486.2005.01097.x>.
- Shuai, Y., Schaaf, C., Zhang, X., Strahler, A., Roy, D., Morisette, J., Wang, Z., Nightingale, J., Nickeson, J., Richardson, A.D., Xie, D., Wang, J., Li, X., Strabala, K., Davies, J.E., 2013. Daily MODIS 500 m reflectance anisotropy direct broadcast (DB) products for monitoring vegetation phenology dynamics. *Int. J. Remote Sens.* 34, 5997–6016. <http://dx.doi.org/10.1080/01431161.2013.803169>.
- Sonnentag, O., Hufkens, K., Teshera-Sterne, C., Young, A.M., Friedl, M., Braswell, B.H., Milliman, T., O'Keefe, J., Richardson, A.D., 2012. Digital repeat photography for phenological research in forest ecosystems. *Agric. For. Meteorol.* 152, 159–177. <http://dx.doi.org/10.1016/j.agrformet.2011.09.009>.
- Sork, V.L., Aitken, S.N., Dyer, R.J., Eckert, A.J., Legendre, P., Neale, D.B., 2013. Putting the landscape into the genomics of trees: approaches for understanding local adaptation and population responses to changing climate. *Tree Genet. Genomes* 9, 901–911. <http://dx.doi.org/10.1007/s11295-013-0596-x>.
- Stoy, P.C., Williams, M., Disney, M., Prieto-Blanco, A., Huntley, B., Baxter, R., Lewis, P., 2009. Upscaling as ecological information transfer: a simple framework with application to Arctic ecosystem carbon exchange. *Landsc. Ecol.* 24, 971–986. <http://dx.doi.org/10.1007/s10980-009-9367-3>.
- Toomey, M., Friedl, M.A., Frolking, S., Hufkens, K., Klosterman, S., Sonnentag, O., Baldocchi, D.D., Bernacchi, C.J., Biraud, S.C., Bohrer, G., Brzostek, E., Burns, S.P., Coursolle, C., Hollinger, D.Y., Margolis, H.A., McCaughey, H., Monson, R.K., Munger, J.W., Pallardy, S., Phillips, R.P., Torn, M.S., Wharton, S., Zerri, M., Richardson, A.D., 2015. Greenness indices from digital cameras predict the timing and seasonal dynamics of canopy-scale photosynthesis. *Ecol. Appl.* 25. <http://dx.doi.org/10.1890/14-0005.1>.
- Verger, A., Filella, I., Baret, F., Peñuelas, J., 2016. Vegetation baseline phenology from kilometer global LAI satellite products. *Remote Sens. Environ.* 178, 1–14. <http://dx.doi.org/10.1016/j.rse.2016.02.057>.
- Vitasse, Y., Delzon, S., Dufréne, E., Pontailler, J.-Y., Louvet, J.-M., Kremer, A., Michalet, R., 2009. Leaf phenology sensitivity to temperature in European trees: do within-species populations exhibit similar responses? *Agric. For. Meteorol.* 149, 735–744. <http://dx.doi.org/10.1016/j.agrformet.2008.10.019>.
- White, M.A., de Beurs, K.M., Didan, K., Inouye, D.W., Richardson, A.D., Jensen, O.P., O'Keefe, J., Zhang, G., Nemani, R.R., van Leeuwen, W.J.D., Brown, J.F., de Wit, A., Schaepman, M., Lin, X., Dettinger, M., Bailey, A.S., Kimball, J., Schwartz, M.D., Baldocchi, D.D., Lee, J.T., Lauenroth, W.K., 2009. Intercomparison, interpretation, and assessment of spring phenology in North America estimated from remote sensing for 1982–2006. *Glob. Change Biol.* 15, 2335–2359. <http://dx.doi.org/10.1111/j.1365-2486.2009.01910.x>.
- Wingate, L., Ogée, J., Cremonese, E., Filippa, G., Mizunuma, T., Migliavacca, M., Moisy, C., Wilkinson, M., Moureaux, C., Wohlfahrt, G., Hammerle, A., Hörtnagl, L., Gimeno, C., Porcar-Castell, A., Galvagno, M., Nakaji, T., Morison, J., Kolle, O., Knohl, A., Kutsch, W., Kolari, P., Nikinmaa, E., Ibrom, A., Gielen, B., Eugster, W., Balzarolo, M., Papale, D., Klumpp, K., Köstner, B., Grünwald, T., Joffre, R., Ourcival, J.-M., Hellstrom, M., Lindroth, A., George, C., Longdoz, B., Genty, B., Levula, J., Heinesch, B., Sprintsin, M., Yakir, D., Manise, T., Guyon, D., Ahrends, H., Plaza-Aguilar, A., Guan, J.H., Grace, J., 2015. Interpreting canopy development and physiology using a European phenology camera network at flux sites. *Biogeosciences* 12, 5995–6015. <http://dx.doi.org/10.5194/bg-12-5995-2015>.
- Woodcock, C.E., Strahler, A.H., 1987. The factor of scale in remote sensing. *Remote Sens. Environ.* 21, 311–332. [http://dx.doi.org/10.1016/0034-4257\(87\)90015-0](http://dx.doi.org/10.1016/0034-4257(87)90015-0).
- Yang, X., Tang, J., Mustard, J., 2014. Beyond leaf color: comparing camera-based phenological metrics with leaf biochemical, biophysical and spectral properties throughout the growing season of a temperate deciduous forest. *J. Geophys. Res.* Biogeosci. 119, 181–191. <http://dx.doi.org/10.1002/2013JG002460>.
- Zhang, X., Friedl, M.A., Schaaf, C.B., Strahler, A.H., Hodges, J.C.F., Gao, F., Reed, B.C., Huete, A., 2003. Monitoring vegetation phenology using MODIS. *Remote Sens. Environ.* 84, 471–475. [http://dx.doi.org/10.1016/S0034-4257\(02\)00135-9](http://dx.doi.org/10.1016/S0034-4257(02)00135-9).
- Zhang, X., Friedl, M.A., Schaaf, C.B., 2006. Global vegetation phenology from Moderate Resolution Imaging Spectroradiometer (MODIS): evaluation of global patterns and comparison with in situ measurements. *J. Geophys. Res.* Biogeosci. 111. <http://dx.doi.org/10.1029/2006JG000217>.